RESEARCH ARTICLE

Development and Validation of a Calculation Routine for the Precise Determination of Pulse Overlap and Accumulated Fluence in Pulsed Laser Surface Treatment

Tobias Fox* and Frank Mücklich

In laser material processing, a variety of parameters like pulse fluence, total dose, step size, and pulse-to-pulse overlap are used to define and compare laser processes. Of these parameters, the pulse-to-pulse overlap can be the hardest to access as it is not implemented directly but instead depends on the spot diameter, its shape, and the respective scanning path that is used to cover the surface. This article shows that existing calculation routes overestimate the actual overlap by up to 21%. A novel calculation route is developed that greatly facilitates the determination of the pulse overlap and thereby the average number of laser pulses that interact with a given point on the surface. This approach makes it possible to achieve more reliable and comparable laser processes, which in return leads to better control of the procedure as the effect of individual parameters on a given output can be determined with greater precision.

1. Introduction

The overlapping of circular laser spots plays a crucial role in laser surface functionalization where homogeneous surface coverage is required.[1–6] Other techniques like cutting, welding, and 3D manufacturing using pulsed lasers also require the scanning of surfaces and consequently, the overlap of multiple laser spots. This is generally achieved by overlapping multiple uniaxial scan lines consisting of individual spots with a defined line-to-line distance, the so-called hatching distance, until the desired surface is covered. The total pulse-to-pulse overlap resulting from the overlaps in both scan directions marks one of the most important parameters in laser processing as it describes the average number of pulses that interact with a given point on the surface. Together with the pulse fluence, the total overlap is generally altered systematically to perform parameter

T. Fox, F. Mücklich
Chair of Functional Materials
Saarland University
Campus D3.3, Saarbrücken 66123, Germany
E-mail: tobias.fox@uni-saarland.de

The ORCID identification number(s) for the author(s) of this article can be found under https://doi.org/10.1002/adem.202201021.

screenings to characterize and optimize processes. Consequently, it is crucial that the overlap is calculated and reported correctly to ensure flawless experiments and comparability. However, as the pulse overlap depends strongly on the spot shape and the employed scanning routine, its calculation can be challenging.[7–15]

The impact of the applied scanning routine on the quality of a resulting surface is especially evident in the case of direct laser interference patterning (DLIP). This is because this technique produces an interference-based periodic pattern within the individual scan lines.[16] If the hatching distance (Δy) between these scan lines is too large the surface modulation caused by the Gaussian profile of the laser beam can cause a superimposed periodicity as shown in **Figure 1**.

To avoid periodic surface modulation, the hatching distance is usually reduced until the outer regions of each scan line overlap sufficiently to form a homogeneous surface. The pulse-to-pulse overlap (OL) thereby defines the number of pulses n_x interacting with a given point in the surface and is generally calculated using Equation (1), where Δx refers to the step size within the scan line according to Figure 1 and D refers to the respective spot diameter.

$$\text{OL} = \left(1 - \frac{\Delta x}{D}\right) \times 100 = (1 - 1/n_x) \times 100 \tag{1}$$

However, as this equation only considers the overlap within a single scan line (given by Δx) and not the overlap of separate lines (given by Δy) there is an intrinsic error that leads to an underestimation of the overlap. This effect is relatively small if the overlap in the x-direction is significantly greater than the one in the y-direction, but it becomes significant if the overlap between lines is increased. [1,4,17]

Additionally, if the overlap in the y-direction is increased the overlap in the x-direction must be decreased respectively to keep the overall overlap constant. This, however, leads to the second cause of the error as Equation (1) can only be used for rectangular spots or as an approximation for circular spots with step sizes that are relatively small compared to the spot radius r. For bigger step sizes the overlap of two circular spots is instead described more accurately by Equation (2).[18,19] While Equation (2) can be used to calculate the overlap within one scan line for a given step size Δx, it also does not consider the overlap of different
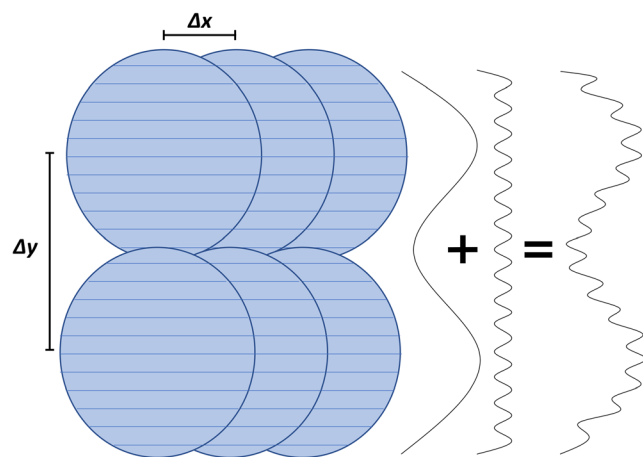
Figure 1. Schematic surface scan in which the hatching distance Δy is too large resulting in a periodical surface modulation in addition to the desired interference pattern.

scan lines and most importantly, cannot be solved for Δx. Therefore, Equation (2) cannot be used to calculate the step sizes that are required to achieve the desired overlap. Especially, if the y-direction is considered as well approximating Equation (2) and solving the approximation for Δx is unfeasible.

$$\text{OL} = \frac{2 \times r^2 \times \cos^{-1}\left(\frac{\Delta x}{2r}\right) - \frac{\Delta x}{2} \times \sqrt{4 \times r^2 - \Delta x^2}}{\pi \times r^2} \times 100 \quad (2)$$

The following section describes a calculation route that aims to avoid the described errors and makes it possible to calculate the spot overlap for a wide variety of spot profiles. This further makes it possible to calculate the spot overlap and accumulated fluence on a processed area even if the hatching distance is reduced. This generally leads to a more even surface coverage and a more homogenous intensity distribution. The approach is then verified in two experiments for which titanium was chosen as reference material. Titanium was chosen because it is widely used in applications that require precise surface treatments like aerospace and biomedicine and because of its use in additive manufacturing that also requires defined scanning routines.[20–23] For those reasons, a significant amount of research on laser processing of this material has already been conducted and reported. Comparing these results can, however, oftentimes be challenging as many publications miss crucial details, like the used spot diameter, when describing the experimental setup or do not clearly describe how a stated overlap was calculated. If the overlap is calculated, it is generally done using Equation (1) which comes with the aforementioned intrinsic errors as it assumes rectangular spots and does not consider the overlap between scan lines.[24–32] With that in mind, this work proposes a relatively simple and straightforward calculation route that could, when implemented widely, greatly improve the comparability and reproducibility of experiments across various fields of research and facilitate the transfer to industry.

2. Results and Discussion

The following section presents a detailed derivation that leads to a set of equations that can be used to determine crucial process parameters such as pulse overlap, accumulated fluence, or the required step sizes needed to achieve the desired number of laser pulses per point in the surface. The model is then validated using ultra short pulsed DLIP on titanium surfaces.

2.1. Formalism Development

To start the calculation a rectangular reference surface A_{ref} with

$$A_{\text{ref}} = x_{\text{ref}} \times y_{\text{ref}} \quad (3)$$

can be assumed. With given pulse distances Δx and Δy the total number of pulses n_{ref} applied to this reference area is defined by Equation (4).

$$n_{\text{ref}} = \frac{x_{\text{ref}}}{\Delta x} \times \frac{y_{\text{ref}}}{\Delta y} \quad (4)$$

The accumulated fluence F_{acc} on the reference surface is then given by the single pulse energy E_{Pulse}, the number of pulses and the reference area according to Equation (5).

$$F_{\text{acc}} = \frac{E_{\text{Pulse}} \times n_{\text{ref}}}{A_{\text{ref}}} \quad (5)$$

Equation (5) can then be combined with Equation (4) to eliminate the reference values and achieve Equation (6).

$$F_{\text{acc}} = \frac{E_{\text{Pulse}}}{\Delta x \times \Delta y} \quad (6)$$

It is important to note that Equation (6) does not rely on the spot area or shape and can therefore be used without requiring the complex calculation of overlap areas as in Equation (2).

The total number of pulses n_{acc} by which the accumulated fluence is applied on a given point of the surface can be calculated with Equation (7) and is then used to calculate the averaged pulse overlap (OL) via Equation (8).

$$n_{\text{acc}} = \frac{F_{\text{acc}}}{F_{\text{Pulse}}} = \frac{F_{\text{acc}} \times A_{\text{Spot}}}{E_{\text{Pulse}}} \quad (7)$$

$$\text{OL}(\%) = (1 - 1/n_{\text{acc}}) \times 100 \quad (8)$$

In contrast to Equation (2), this set of equations can easily be solved for Δx meaning that the necessary pulse distance required to achieve the desired overlap can be calculated. This greatly facilitates parameter screenings that aim to systematically vary the pulse overlap.

An example of the calculation of process parameters using these equations is given in the experimental section. As can be seen from Equation (7), the area of a single laser spot A_{Spot} is required for the last calculation step. While for Gaussian beam profiles, this value can be easily determined mathematically, in the case of more complex beam profiles it is recommended to first observe the effective spot diameter with the desired pulse fluence on the surface. Apart from the spot area, the transversal

**ADVANCED
SCIENCE NEWS**
www.advancedsciencenews.com

**ADVANCED
ENGINEERING
MATERIALS**
www.aem-journal.com

beam profile is not considered any further as the objective of the scanning routine is to achieve homogenous surface coverage and thereby even out the intensity distribution. Therefore, only the average values are considered.

2.2. Experimental Validation

The approach derived in Section 2.1 was validated in two separate experiments. This was done using the USP-DLIP setup described in Ref. [2] employing a titanium–sapphire femtosecond laser with a pulse duration of 100 fs and a repetition rate of 1 kHz. This setup ensures that heat accumulation within a scan line and between different scan lines is neglectable as it can be assumed that the material reaches equilibrium before the next pulse arrives. The periodicity of the applied interference pattern was fixed to 3 μm. Further details on the patterning method and the setup used are given in the experimental section.

2.2.1. Validation of a Model Surface

To cover a surface with a defined average number of pulses per point (n_{acc}), the required step sizes in the x- and y-directions need to be calculated, respectively. The following section illustrates the shortcomings of state-of-the-art approaches to do so and investigates the newly developed model.

A scan with an average surface coverage of one pulse per point on the surface was performed. In case of spherical spots, where a surface coverage without gaps is not possible, this task requires some spot overlap. This way, if the surface area without any laser interaction is equal to the area with two interactions, each point on the surface experiences an average of one interaction. The average pulse number of one pulse per point was chosen due to the simplicity of evaluation of the resulting surfaces (**Figure 2**) and because this example shows that the widely established approach of employing Equation (1) to calculate the fluence fails to consider the free spaces between non-rectangular spots. Instead, if Equation (1) is applied to the same problem, the result would be a step size equal to the beam diameter resulting in a surface with no overlap but significant unirradiated areas.

In contrast to Equation (1), Equation (2) considers the circular shape of the spot. However, it cannot be solved for Δx and the necessity to consider the second scan direction and the respective overlap in Δy makes numeric solutions unfeasible. Additionally, deviations from the circular shape would easily result in errors while the newly developed method only requires the spot area regardless of shape.

To verify that the proposed calculation route can determine the step sizes in the x- and y-directions, the surface depicted in Figure 2a was produced. The spot diameter was 79 μm resulting in step sizes in the x- and y-directions of 70 μm. While the step sizes in the x- and y-directions do not need to be equal, the calculation was adapted to meet this condition. The detailed calculation is given in the experimental section.

The produced surface is depicted in Figure 2a and appears to be close to the ideal arrangement of spots in Figure 2d. To determine the surface fractions that interacted with 0, 1, or 2 pulses
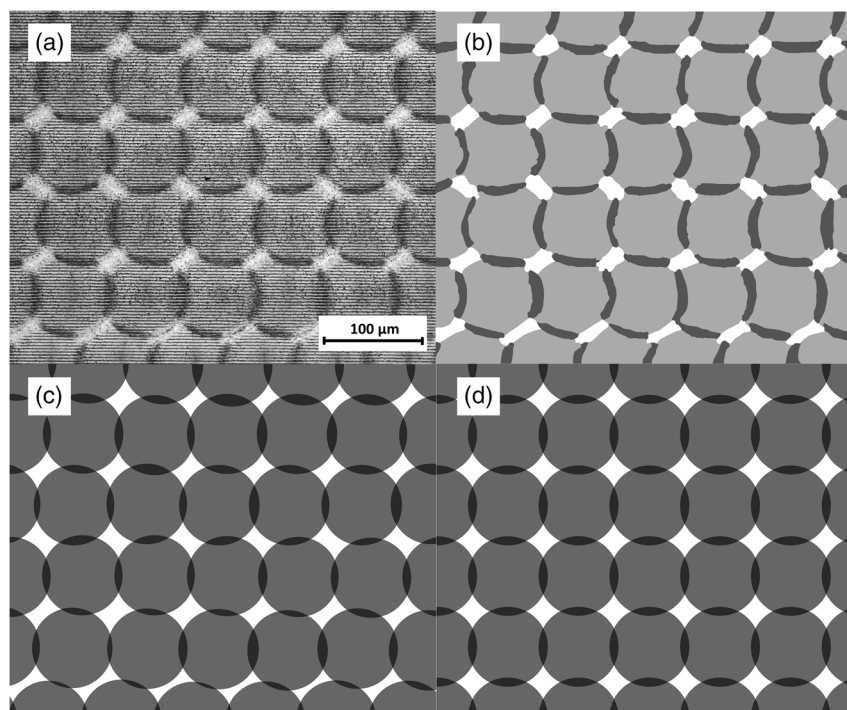

Figure 2. a) Laser scanning microscope picture of the produced surface with a spot diameter of 79 μm and a desired step size of 70 μm in the x- and y-directions. b) Segmentation of image a) to determine the surface fractions that experienced one (light gray), two (dark gray) or zero (white) laser interactions. c) Approximating a) with circles to determine the idealized surface area fractions. d) Ideal grid for step sizes of 70 μm.

2201021 (3 of 7)

**ADVANCED
SCIENCE NEWS**

www.advancedsciencenews.com

**ADVANCED
ENGINEERING
MATERIALS**

www.aem-journal.com

the image was segmented manually as shown in Figure 2b. Additionally, circles were fitted to the spots in (a) to determine idealized surface fractions for the real surface.

The images (b) to (d) were analyzed via image analysis to obtain the regions of the surface that interacted with 0, 1, or 2 pulses. This was done by employing a grayscale threshold, where the bright areas represent 0 interactions, the gray areas 1 interaction, and the dark areas 2 interactions. The results are given in **Table 1**.

It becomes evident that the results for the ideal grid meet the expectation that the area affected by two pulses is equal to that affected by 0 pulses, resulting in an average of one interaction per point on the surface as was the premise of the calculation. The results for the idealized surface are close to this result. However, the inaccuracy of the sample stage led to a distortion of the theoretical grid and thereby to a deviation from the theoretical values.

Interestingly, the real surface shows a strong increase in the area subjected to two pulses that cannot be explained by the given model. To explain this result, it must be considered that the patterned regions show a lower ablation threshold than the polished surface as a result of an increased surface roughness, oxidation, and damage accumulation.[2,33,34] This results in an increase in the effective spot diameter in the overlap areas as shown in **Figure 3**, as the outer regions of the beam profile that did not

cause ablation on the polished areas can interact significantly with the already patterned areas. This leads to additional two-pulse areas. While the model only expects the overlap between the black circles showing the formerly measured spot diameter of 79 µm, the apparent spot diameter on the patterned surfaces increases to around 85.2 µm, and additional two-pulse areas between the red circles are produced. When calculating the expected overlap of circles with a diameter of 85.2 µm using Equation (2) and the used step size of 70 µm the resulting 17.6% are relatively close to the measured two-pulse area in the real surface (16.11%). This demonstrates that a correct assessment of the effective spot area is crucial to calculate relevant process parameters.[33–36]

To assess how strongly this additional absorption influences the obtained results, multiple surfaces were produced and systematically analyzed in the next section.

2.2.2. Validation of the Model for Fully Patterned Surfaces

To evaluate the processing parameters on fully patterned surfaces, an exemplary study was carried out, observing the pattern depth of a DLIP line pattern with 3 µm periodicity and its dependence upon the pulse fluence F_{Pulse}, the number of pulses per point n_{acc}, and the step size in y direction Δy. The evaluated factors and the results including the standard deviation of the nine measurements taken per parameter combination are given in **Table 2**. It is expected that Δy has no effect on the pattern depth, as the step size in the y-direction is balanced with a respectively calculated step size in the x-direction to keep n_{acc} on the desired level. Two exemplary surfaces are shown in **Figure 4**.

The data from Table 2 was evaluated using the software "Minitab 19" (Minitab GmbH) to produce the Pareto chart shown in Figure 4. This chart shows to what extent the different input parameters influence the output parameter, i.e., the pattern depth. As expected, the pulse fluence and the number of pulses per point have the strongest influence on the resulting pattern depth. Their interaction also shows a strong effect meaning that the two parameters do not influence the result independently but show a strong synergy. The step size in the y-direction and its interactions with the other parameters shows only a minor effect

Table 1. Surface coverage of the real surface (Figure 2b), its idealized approximation (c), and of the ideal grid (d).

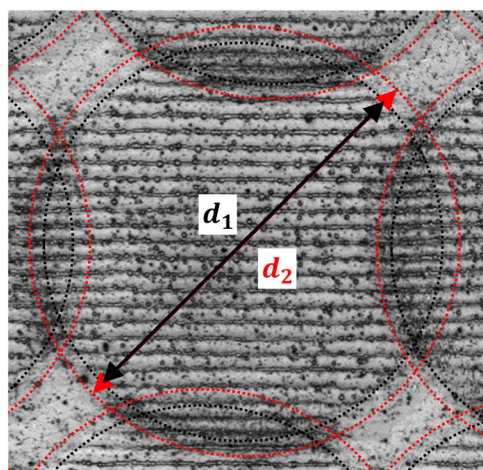|	0 Pulses	1 Pulse	2 Pulses
Real Surface	7.93%	75.96%	16.11%
Idealized Surface	8.96%	83.02%	8.02%
Ideal Grid	9.20%	81.60%	9.20%

Figure 3. Detailed view of one of the spots from Figure 2a. The black circles indicate the spot diameter on the polished surface ($d_1 = 79$ µm) that was used for the calculations. The red circles indicate the increased effective spot diameter ($d_2 = 85.2$ µm) within the patterned regions. This increase in effective spot diameter causes an additional two-pulse overlap (dark regions between red circles) that is not accounted for in the model.

Table 2. Experimental design to investigate the three parameters F_{Pulse}, n_{acc}, and Δy with two levels each. Δx was determined using the model above. The spot diameter was 70 µm. σ refers to the standard deviation of the measured pattern depths.

F_{Pulse} [J cm^{-2}]	n_{acc} -	Δy [µm]	Δx [µm]	Pattern Depth [µm]	σ [µm]
0.5	10	6	64	451.56	27.46
0.5	10	24	16	479.89	30.29
0.5	20	6	32	800.56	21.43
0.5	20	24	8	801.67	55.91
1	10	6	64	884.44	77.38
1	10	24	16	1070.44	50.42
1	20	6	32	1804.56	141.82
1	20	24	8	1849.56	97.71

**ADVANCED
SCIENCE NEWS**

www.advancedsciencenews.com

**ADVANCED
ENGINEERING
MATERIALS**

www.aem-journal.com
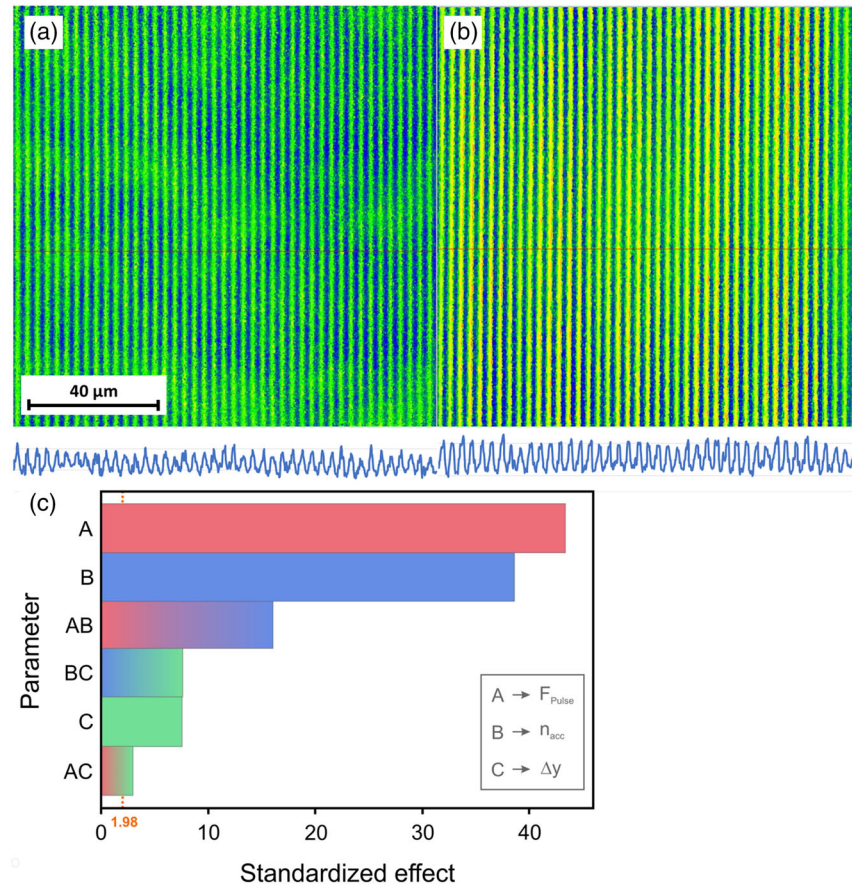
Figure 4. a) Exemplary surface with $F_{Pulse} = 0.5\,\mathrm{J\,cm^{-2}}$, $n_{acc} = 10$, and $\Delta y = 6\,\mu m$. The profile scan has a scale from 0 to 1.5 µm. b) Exemplary surface with $F_{Pulse} = 1\,\mathrm{J\,cm^{-2}}$, $n_{acc} = 20$ and $\Delta y = 24\,\mu m$. The profile scan has a scale from 0 to 4 µm. c) The Pareto chart for the given data set shows that the pulse fluence and the number of pulses have a strong effect on the resulting pattern depth. The interaction between those two factors also influences the depth strongly. The weakest effects are associated with Δy meaning that this factor has very little influence on the resulting depth.

that is, however, not below the significance threshold of 1.98. This remaining effect of Δy likely originated from the discrepancy between the observed spot diameter on a polished surface and the effective spot diameter within the pattern that was observed in Section 2.2.1.

It should be noted that using Equation (1) to calculate the overlap in the x- and y-direction for the patterns in Table 2 would result in an overestimation of the actual overlap by over 21%. This observation underlines the importance of the correct calculation route to systematically assess the effect of the laser parameters on the resulting surface. Equation (2) gives correct results for circular spots but is restricted in its applicability as it cannot be solved for Δx meaning it cannot be used to calculate the step sizes required to achieve the desired pulse number. In research, a discrepancy between the calculated and the true parameters can have major effects as the main objective of most parameter screenings lies in finding the ideal combination of pulse fluence and overlap that is required to achieve the desired effect. If these values are not calculated or reported correctly other research groups are not able to produce comparable surfaces without repeating the parameter screening themselves. Perhaps more

importantly, errors in the parameter calculation can lead to major difficulties when the laser process is transferred to the industrial application as these transfers generally aim to translate the ideal laser parameters found in the lab to an industrial scale setup that generally employs vastly different input parameters like pulse power, spot size, and frequency. It is therefore crucial that parameters like overlap, pulse fluence, and accumulated fluence are calculated and reported as precisely as possible.

3. Concluding Remarks

The calculation route developed in this contribution allows the straightforward calculation of the spot overlap and the accumulated fluence on an irradiated material's surface with higher precision than established methods. This is especially true for complex scanning paths or non-Gaussian beam profiles as the average number of pulses on a given point of the surface is calculated using only the step sizes and the spot area. This makes it possible to evaluate the influence of single process parameters with greater precision and to compare surfaces that were produced with different parameters or setups. Having access to

the exact process parameters that resulted in a given structure also makes it possible to develop more precise models and make sound predictions for their respective properties. As stated earlier, the alternative of using established methods to calculate the overlap in the x- and y-direction can lead to an error of over 21% in the estimation of the overlap and consequently, the total accumulated fluence on the surface.

The main challenge of the technique lies in the determination of the effective spot size, a requirement for the determination of the pulse fluence. This is because the reference spots on a polished surface, which are generally used to determine the spot size, show a smaller diameter than the spots within the patterned surface, where the material usually shows a lower ablation threshold as a result of oxidation, roughening and damage accumulation. This problem is shared with established calculation routines as they too need to determine the effective spot diameter prior to the patterning.

Future works could employ a scan with bigger step sizes like the scan with one pulse per point conducted in this work to determine the spot diameter within a patterned surface experimentally. Alternatively, a focus on the precise laser-material interaction of the system could enable researchers to quantify the reduction of the ablation threshold caused by the patterning. This way the effective spot size within the patterned area could be accessed even for higher pulse numbers.

4. Experimental Section

Material Preparation: Titanium samples were cut out of a sheet (HMW Hanauer GmbH; 99.995 wt.%) using wire-cut electrical discharge machining (EDM).

The samples were prepared with the following steps: 1) Heat treatment in vacuum ($\approx 10^{-5}$ mbar) at 700 °C for 10 min. (heating/cooling rate: 1 °C min^{-1}). The main purpose of this treatment was to remove surface contaminations and potential thermal influences on the sample edges caused by the EDM. 2) Grinding: The samples were grinded using SiC grinding discs (#600–200 s; #1200–600 s) 3) OPS polishing: OPS + 2% H_2O_2 (30% $_{W/V}$) + 2% NH_3 (25% $_{V/V}$) for 8 min. 4) Etching in Beraha I stock solution for 45 s. This step is used to remove the deformation layer that forms on the Ti surface during the previous steps. 5) OPS polishing identical to three.

The resulting surfaces were cleaned in an ethanol ultrasonic bath for 10 min immediately after the polishing as well as immediately before and after the laser processing.

Laser Processing: The laser patterning was conducted using a Titanium-Sapphire laser with a centered wavelength of 800 nm, a pulse duration of 100 fs, and a repetition rate of up to 1 kHz. Ultrashort pulsed direct laser interference patterning was used to produce a line pattern with a periodicity of 3 μm within the individual laser spots. To achieve this, the main beam is split into two coherent sub-beams that are then brought to interference on the sample surface to create a periodical, line-shaped interference pattern. This pattern is then transferred to the material surface through a combination of direct ablation and thermal processes. Further details on the technique and the setup used can be found in Müller et al.[3] In contrast to a related work,[10] the setup uses a mask to reduce the beam diameter of the Gaussian beam from 8 to 3 mm. This way an approximate top hat profile is achieved.

The set of equations given in Section 2 was fed into an Excel spreadsheet and used to calculate the required structuring parameters. To illustrate this, the calculation process to produce the surface depicted in Figure 2a is given below.

Given parameters:
Spot Diameter: $D = 79$ μm.
Desired number of pulses per point: $n_{acc} = 1$.
Laser Power: $P = 26.7$ mW.
Expected losses in the DLIP system, here: $L = 10\%$.
Laser repetition rate: $f = 250$ Hz.
Additional condition: $\Delta x = \Delta y$.

Generally, this condition is not required. Instead, one of the step sizes can be chosen freely but should generally be a multiple of the DLIP periodicity in the respective direction.

$$E_{Pulse} = \frac{P \times (1 - L)}{f} = 96.12 \, \mu J \tag{9}$$

$$F_{Pulse} = \frac{E_{Pulse}}{A_{Spot}} = 1.96 \, \mu J \, cm^{-2} \tag{10}$$

$$F_{Pulse} = \frac{E_{Pulse}}{\Delta x \times \Delta y} = \frac{E_{Pulse}}{\Delta x^2} \tag{11}$$

$$\Delta x = \Delta y = \sqrt{\frac{E_{Pulse}}{F_{Pulse}}} = 70 \, \mu m \tag{12}$$

Surface Analysis: An OLS4100 confocal laser scanning microscope was used to determine the respective spot diameters and surface profiles. Image segmentation was then performed using the software "Amira" (version 5.3.1). For the simplified images (Figure 2b,c) the image analysis was performed with the software "Gimp".

The analysis of the experimental design (Section 2.2.2) was performed using the software Minitab 19 (Version 2020.1).

Conflict of Interest

The authors declare no conflict of interest.

Data Availability Statement

The data that support the findings of this study are available on request from the corresponding author. The data are not publicly available due to privacy or ethical restrictions.

[1] A. I. Aguilar-morales, S. Alamri, T. Kunze, A. F. Lasagni, *Opt. Laser Technol.* **2018**, *107*, 216.

[2] D. W. Müller, T. Fox, P. G. Grützmacher, S. Suarez, *Sci. Rep.* **2020**, *10*, 1.

[3] M. Mezera, S. Alamri, W. A. P. M. Hendriks, A. Hertwig, A. M. Elert, J. Bonse, T. Kunze, A. F. Lasagni, G. R. B. E. Römer, *Nanomaterials* **2020**, *10*, 1184.

[4] A. J. Antończak, Ł. Skowroński, M. Trzcinski, V. V. Kinzhybalo, Ł.K. Łazarek, K. M. Abramski, *Appl. Surf. Sci.* **2014**, *325*, 217.

[5] B. Voisiat, A. I. Aguilar-Morales, T. Kunze, A. F. Lasagni, *Materials* **2020**, *13*, 1.

[6] S. Milles, M. Soldera, B. Voisiat, A. F. Lasagni, *Sci. Rep.* **2019**, *9*, 1.

[7] C. Leone, S. Genna, A. Caggiano, V. Tagliaferri, R. Molitierno, *Proc. CIRP* **2015**, *28*, 64.

[8] K. L. Wlodarczyk, A. Brunton, P. Rumsby, D. P. Hand, *Opt. Lasers Eng.* **2016**, *78*, 64.

[9] L. Shanjin, W. Yang, *Opt. Lasers Eng.* **2006**, *44*, 1067.

[10] Y. Singh, J. Singh, S. Sharma, A. Sharma, J. Singh Chohan, *Mater. Today Proc.* **2021**, *48*, 1021.

[11] P. Bajaj, J. Wright, I. Todd, E. A. Jägle, *Addit. Manuf.* **2019**, *27*, 246.

[12] S. C. Chou, M. Trask, J. Danovitch, X. L. Wang, J. P. Choi, M. Brochu, *Mater. Charact.* **2018**, *143*, 27.

[13] Y. Lo, B. Liu, H. Tran, *Int. J. Adv. Manuf. Technol.* **2019**, *105*, 2989.

[14] N. Singh, P. Hameed, R. Ummethala, G. Manivasagam, K. G. Prashanth, J. Eckert, *Mater. Today Adv.* **2020**, *8*, 100097.

[15] A. Ghosh, D. Misra, S. K. Acharyya, *Lasers Manuf. Mater. Process.* **2019**, *6*, 228.

[16] A. F. Lasagni, C. Gachot, K. E. Trinh, M. Hand, A. Rosenkranz, T. Roch, S. Echhardt, T. Kunze, M. Bieda, D. Günther, V. Lang, F. Mücklich, in *Laser-Based Micro- and Nanoprocessing* Vol. *XI*, San Diego Convention Center, San Diego, California, United States **2017**, p. 1009211.

[17] M. K. Mohammed, U. Umer, O. Abdulhameed, H. Alkhalefah, *Appl. Sci.* **2019**, *9*, 1.

[18] J. Jiménez, Á. Gómez, M. D. Buhrmester, V. Alexandra, W. Harvey, W. B. Swann, *Soc. Sci. Comp. Rev.* **2015**, *5*, 215.

[19] E. W. Weisstein, *Mathworld.Wolfram.Com,* **2022**, https://mathworld.wolfram.com/Circle-CircleIntersection.html (accessed: May 2022).

[20] M. Liu, R. Zhou, Z. Chen, H. Yan, J. Cui, W. Liu, J. H. Pan, M. Hong, *Coatings* **2020**, *10*, 450.

[21] X. Miao, M. Wu, J. Han, H. Li, X. Ye, *Materials* **2020**, *13*, 3940.

[22] C. Zwahr, D. Günther, T. Brinkmann, N. Gulow, S. Oswald, *Adv. Healthc. Mater.* **2017**, *6*, 1.

[23] C. Zwahr, R. Helbig, C. Werner, A. F. Lasagni, *Sci. Rep.* **2019**, *9*, 1.

[24] C. Florian, R. Wonneberger, A. Undisz, S. V. Kirner, K. Wasmuth, D. Spaltmann, J. Krüger, J. Bonse, *Appl. Phys. A: Mater. Sci. Proc.* **2020**, *126*, 1.

[25] A. Peter, A. H. A. Lutey, S. Faas, L. Romoli, V. Onuseit, T. Graf, *Opt. Laser Technol.* **2020**, *123*, 105954.

[26] F. Schell, S. Alamri, A. Hariharan, A. Gebert, A. F. Lasagni, T. Kunze, *Mater. Lett.* **2022**, *306*, 130920.

[27] L. Gemini, M. Faucon, L. Romoli, R. Kling, in *Laser-Based Micro- and Nanoprocessing*, Vol. *XI*, San Diego Convention Center, San Diego, California, United States **2017**, p. 10092.

[28] A. H. A. Lutey, L. Gemini, L. Romoli, G. Lazzini, F. Fuso, M. Faucon, R. Kling, *Sci. Rep.* **2018**, *8*, 1.

[29] C. Du, C. Wang, T. Zhang, L. Zheng, *ACS Appl. Bio Mater.* **2021**, *5*, 272.

[30] H. Zhu, M. Ehrhardt, P. Lorenz, J. Zajadacz, J. Lu, K. Zimmer, *Appl. Phys. A: Mater. Sci. Proc.* **2019**, *125*, 1.

[31] K. Yin, H. Du, X. Dong, C. Wang, J. A. Duan, J. He, *Nanoscale* **2017**, *9*, 14620.

[32] I. Gnilitskyi, T. J. Y. Derrien, Y. Levy, N. M. Bulgakova, T. Mocek, L. Orazi, *Sci. Rep.* **2017**, *7*, 1.

[33] P. T. Mannion, J. Magee, E. Coyne, G. M. O'Connor, T. J. Glynn, *Appl. Surf. Sci.* **2004**, *233*, 275.

[34] F. Di Niso, C. Gaudiuso, T. Sibillano, F. P. Mezzapesa, A. Ancona, *Phys. Proc.* **2013**, *41*, 698.

[35] S. E. Kirkwood, A. C. Van Popta, Y. Y. Tsui, R. Fedosejevs, *Appl. Phys. A: Mater. Sci. Proc.* **2005**, *81*, 729.

[36] L. M. Machado, R. E. Samad, W. De Rossi, N. Dias, *Opt. Express* **2012**, *20*, 4114.